

# Torque Ripple Reduction in an Axial Flux High Temperature Superconducting Motor

A. González-Parada, F. Trillaud, R. Guzmán-Cabrera, M. Abatal

**Abstract**—The design, construction and operation of superconducting rotatory machines in axial flux configuration is strongly dependent on the ability to reduce torque ripple. A new concept is presented in order to maximize the output power optimizing the magnetic flux density within the air gap of a three-phase fully superconducting induction motor. The machine is designed on a basis of bilateral stators distributed around a central rotor. The optimal distribution of magnetic flux and the minimization of torque ripple are resulting from an adequate distribution of motor phases, number of rotor bars and choice of air gap thickness. The magnitude of magnetic flux in the air gap is obtained by means of finite element analysis and some derived parameters are compared to experimental results. Then, the impact of the design on torque magnitude and torque ripple is discussed.

**Index Terms**— Air gap magnetic flux density, Axial flux machine, HTS motors, torque ripple.

## I. INTRODUCTION

THE main characteristics of Axial Flux Machines (AFM) are twofold: (1) the magnetic field is aligned with the axis of the electrical machine and (2) the active current in conductors is radial. Due to their planar configuration, the air gap between stator and rotor can be adjusted, and greater power to weight and diameter to length ratios as well as compacter constructions with higher efficiency can be achieved [1], [2]. These advantages have led to numerous research studies to introduce High Temperature Superconductor (HTS) technology into AFM's [2]-[4]. Most of these studies focused on the design and construction of hysteresis and reluctance motors using YBCO bulk parts made of single piece or several disks uniformly distributed around the rotor [3]. Thus, replacing permanent magnets for field-cooled bulk YBCO materials allows increasing the magnetic field in the air gap and achieve compacter full superconducting machines [5].

The following article presents a new concept replacing bulk materials by an assembly of HTS tapes as part of the development of a hysteresis AFM. In the proposed design, the resulting torque results from the interaction of the currents induced in the superconducting tapes and the magnetic flux

density created by the stator. One of the drawbacks of this configuration is the production of an undesired torque ripple affecting the machine performance, which results from the distortion of the magnetic flux density in the air gap. Many techniques for torque ripple minimization are documented in literature [6], [7]. These techniques include magnet pole shaping, air gap length adjustment, pole to arc ratio and slot less configurations, amongst others. All of these optimization processes may be applied to AFM's, considering the manufacturing costs and production method as well [4]-[7]. Avoiding bulk material yields some advantages against the loss of field density and the necessary presence of additional dissipation due mainly to splices. Thus, in addition to bringing simpler assembly procedure and greater mechanical stability, the principal advantage is the absence of demagnetization effects against induced heat loads in AC operation affecting the overall performance of HTS bulks in electrical machines [8], [9].

The present work focuses on the construction and operation of a full superconducting AFM based on Bi2223 tapes operated at 77.3 K in liquid nitrogen applying design rules and using a preliminary numerical model to help in choosing the best stator-to-rotor configuration. Measurements of torque ripple have been conducted to show the influence of some key design parameters on results.

## II. BASIC DESIGN PARAMETERS

### A. Optimum magnetic flux in air gap and torque ripple

An estimation of torque ripple, taking into account change of total stored energy in the air gap considering the rotor position, may be given by the following relation [4]:

$$T_{Ripple} = \frac{2p}{\pi} mNk_w \Phi I_a \quad (1)$$

where  $\Phi$  is the air gap magnetic flux,  $I_a$  is the stator current,  $p$  is the pole number,  $m$  is phase number,  $N$  is the number of turns in series per phase, and  $k_w$  is the winding factor defined as the product of the distribution factor ( $k_d$ ) and the pitch factor ( $k_p$ ).

To compute the torque ripple, it is necessary to assess the amount of magnetic flux crossing the air gap. The axial flux density in any point along the axial length in the motor can be calculated by means of (2), assuming  $\lambda \ll r$ , as follows [7]:

$$B_\lambda = \frac{\mu_0 e_{mmf}}{\lambda} \sin \frac{p}{2} \theta \quad (2)$$

This work was supported by the CONACYT under Grant 081377.

A. Gonzalez-Parada is with the University of Guanajuato, Mexico (e-mail:gonzalez@ugto.mx)

F. Trillaud is with the Engineering Institute of the National Autonomous University of Mexico, Mexico (e-mail: ftrillaudp@gmail.com).

R. Guzman-Cabrera is with the University of Guanajuato, Mexico (e-mail: guzmanc@ugto.mx).

M. Abatal is with Carmen Autonomous University, Mexico (e-mail: mabatal@pampano.unacar.mx).

where  $e_{\text{mmf}}$  is the magnetomotive force and  $\lambda$  is the air gap thickness as depicted in Figure 1.

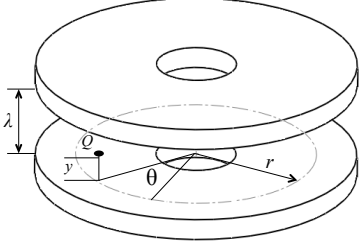


Fig. 1. Parameter distribution in an Axial Flux Machine.

From (2) and assuming a constant magnetic flux density per pole, the corresponding magnetic flux per pole can be estimated as follows [1]:

$$\Phi_{\text{pole}} = \left( \frac{D_o^2}{D_i^2} - 1 \right) \frac{D_i^2}{4p} B_{\lambda} \quad (3)$$

where  $D_o$  is the outer diameter,  $D_i$  is the inner diameter, and  $B_{\lambda}$  is the approximated magnetic flux density in the air gap for a given thickness  $\lambda$ . The ratio  $(D_o/D_i)$  is used to optimize the air gap magnetic flux taking into account the phase number, current and geometric constructions [6], [7], [10], [11].

### B. Rules applied to design the rotor cage

Several authors [12]-[23] showed that for a given number of phases, various feasible pole and slot number combinations exist. If  $S_s$  is the number of slots in the stator and  $S_r$  is the number of slots in the rotor, or in the present case, the number of radial tapes, the selection should consider the following requirements:

1. To avoid noise and vibrations, the relation between  $S_s$  and  $S_r$  must be such that  $S_s - S_r \neq \{\pm 1, \pm 2, \pm(p \pm 1), \pm(p \pm 2)\}$ .
2. To avoid deadlocks and peaks in the starting current, the difference  $S_s - S_r$  must be different from any multiples of  $3p$ .
3. To avoid peaks in par-velocity curve,  $S_s - S_r$  must be different from  $\pm p, -2p$  or  $-5p$ .
4.  $S_r$  must be different to any odd numbers of rotor bars.

Other design parameters such as magnetic field distribution, slot opening air gap length, pole-arc-to-pole pitch ratio, etc., may be taken into account as well. Amongst the diverse parameters affecting the machine performance of squirrel cage rotors, the slot number and pole number combinations represent a good indication of its ripple characteristic. In practice, not all the conditions can be met, but most of them may be taken in account to some extent, especially when the motor has a small number of poles.

## III. MOTOR DESIGN DETAIL AND CONSTRUCTION

### A. General Characteristics of motor and HTS tape

The motor is constituted of two bilateral stators surrounding a squirrel cage-like rotor. Salient parameters of the HTS stator and rotor, both made of Bi2223, are given in table. The resistance per splice is computed from the  $V-I$  curve as presented in [24].

TABLE I  
HTS MOTOR GENERAL CHARACTERISTICS

Description	Characteristics
HTS Tape	BSCCO-2223
Phase number	3
Pole number	8
Operation Voltage	220 V
Frequency	60 Hz
Nominal Speed	180 rpm
Critical Current ( $I_c$ )	100A*
Construction	Two bilateral stators, one central rotor
External diameter	165 mm
Air gap	3 mm
Resistance per splice/phase	$11.4 \times 10^{-3} \Omega$
Total number of splices/phase	32
AC total losses	8.42 kW**

\* $I_c$  determined after the welding process of the HTS tapes [24]

\*\* Operated under critical current value.

Figure 2 gives a general overview of the motor. The upper phases of the stator are labeled 1a to 1c while 1f to 1d correspond to the lower ones. The rotor is labeled 2. Additional design details of the stator and rotor follow.

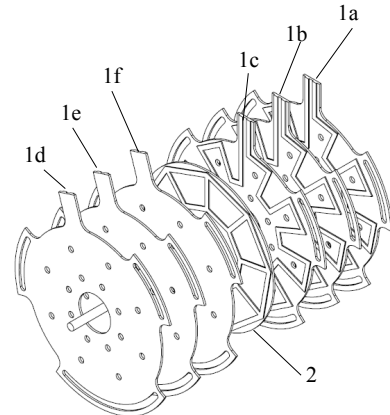


Fig. 2. Distribution of the HTS axial flux motor; 1a to 1c for lower stator phases, 1d to 1f for upper stator phases, and 2 for the central rotor.

**B. Stator**

The construction of the stator was carried out by cutting and soldering HTS tapes so as to achieve the proposed geometry shown in figure 3, thereby avoiding tape bending. This process introduced a reduction in  $I_c$  of about 15% [24].

After soldering the tapes together using solder Sn (60%)-Ag (40%), the assembly was embedded in epoxy resin to achieve mechanical support. Table 2 summarizes the resulting dimensions of both upper and lower stators.

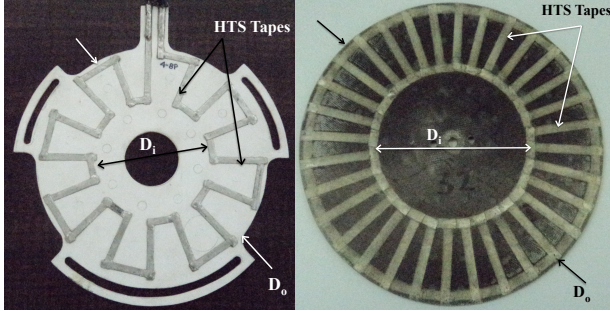


Fig. 3. On the left, detail construction of each phase of the upper and lower stators; on the right, the rotor.

TABLE II  
STATOR GENERAL DIMENSIONS

Description	Dimension
Outer Diameter ( $D_o$ )	157 mm
Inner Diameter ( $D_i$ )	80 mm
$D_o/D_i$ relation	0.4
Number of slots	48

Figure 4 shows an overview of the electrical connections following a delta connection. These connections were chosen considering the phase displacement between the upper and lower stator. The zero position is given by the alignment of the radial tapes of the upper and lower stator.

**C. Rotor**

The rotor cage was designed to be as close as possible of a disk-like shape. This geometrical configuration allows maximizing the actual amount of magnetic flux crossing the rotor poles. The rotor then made of 32 radial branches short-circuited by azimuthal tapes at the inner and outer diameter with the same  $D_o/D_i$  ratio as of the stators in order to have the greater magnetic coupling between stator and rotor. Fig. 5 shows the general rotor construction.

Considering the steady state performance in the motor a 2D Finite Element Analysis (FEA) was performed computing the magnetic flux density in the air gap considering in first approximation the sole contribution of the radial tapes. This simplified model served as basis to find the optimum design parameters of the motor.

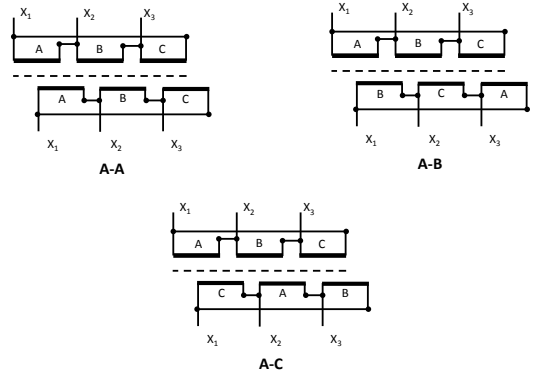


Fig. 4. Configuration of phase connections labeled A-A, A-B, A-C.

**IV. FEA BASE DESIGN**

For this preliminary study, the phase distribution was shuffled around in order to obtain best magnetic coupling between rotor and stator with the smallest distortion of the magnetic flux density at the air gap. The phase distribution follows Fig. 4 and Fig. 5 shows details of phase distribution. A comparative study was performed to determine the best possible configuration amongst the different connections A-A, A-B and A-C.

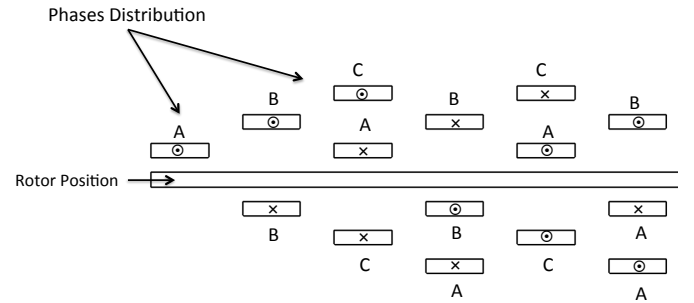


Fig. 5. General overview of the A-B connection performed for 2D FEA simulation.

**V. FINITE ELEMENT ANALYSIS**

**A. 2D FEA simulations**

A preliminary 2D magnetostatic model based on a potential vector formulation was implemented using the open-source software FEMM, solving [25]:

$$\nabla \times \left( \frac{1}{\mu_0} \nabla \times \mathbf{A} \right) = \mathbf{J}_e \tag{4}$$

where is  $J_e$  the current density in the stator. The model does not yet include the induction in the rotor and was mainly used at the time to crosscheck the analytical results obtain with (2) and (3) and determine the best phase configuration as part of the design efforts. Fixing the potential vector equal to 0 at the boundary layer of the model, the solution  $\mathbf{A}(x, y, z, t)$  is obtained over the entire model. The magnetic flux density was then derived on one of the radial tape of rotor using:

$$\mathbf{B} = \nabla \times \mathbf{A} \quad (5)$$

Figure 6 shows the magnetic flux density calculated for an air gap thickness  $\lambda$  equal to 3 mm and the phase configuration A-B following the connection as depicted in Fig. 4. The magnetic flux density per unit length is then computed over each rotor pole, which allows estimating the static torque.

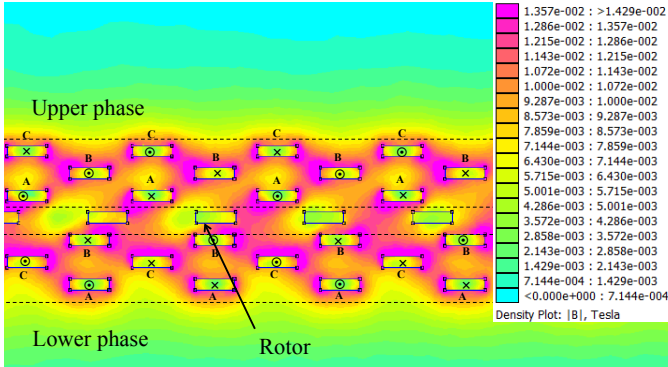


Fig. 6. FEA of Magnetic flux density in Teslas for A-B phase connection including the presence of the rotor.

### VI. TEST RESULTS

To evaluate the torque performance, the HTS motor was coupled to a DC drive and the torque produced by the motor was recorded by a DAQ system as depicted in Fig. 7.

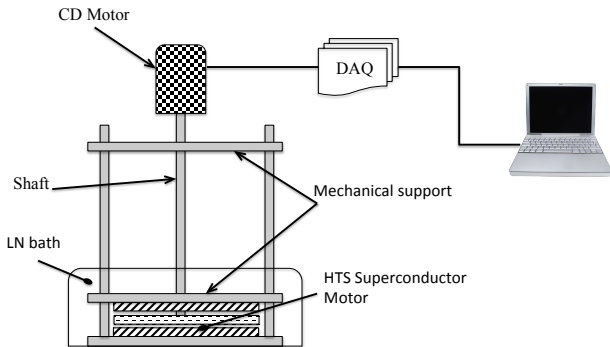


Fig. 7. General test setup to evaluate the torque performance of the HTS motor.

The magnitude of the air gap magnetic flux density directly affects the torque level whereas its harmonic content is responsible torque ripples as discussed in [26]. Fig. 8 shows the magnetic flux density in the rotor depending on phase connections. The biggest distortion occurs in configurations A-A and A-C leading to a waver signal of lower magnitude. Those experimental results were compared with computational ones as given in Fig. 6 showing good agreement despite the model simplifications yielding a measured 0.08 Nm against a computed value equal to 0.07 Nm.

Configuration A-B gives a more stable magnetic flux in the pole, producing a higher torque at minor torque ripples as depicted by figure 9 and 10, the latter showing the ripple torque depending of rotor position and the ripple variation of function of phase connection.

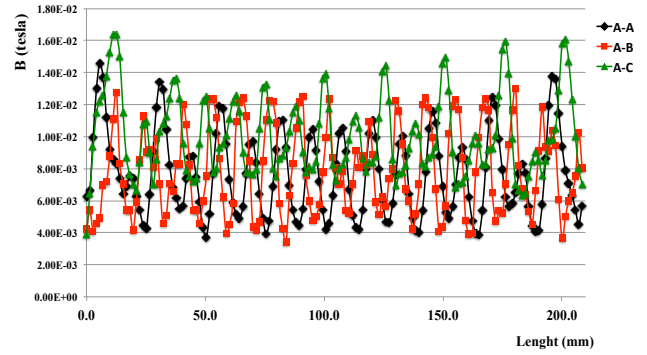


Fig. 8. Magnetic flux density for each phase connection measured on the rotor.

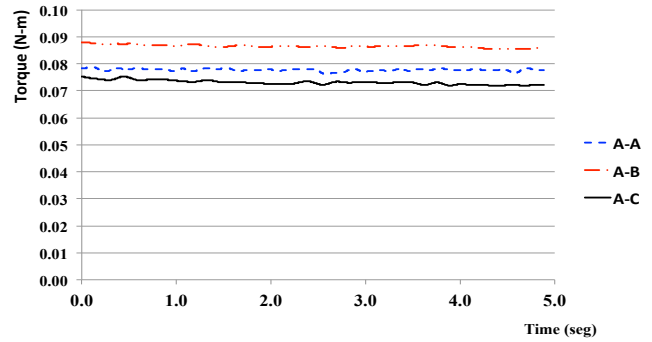


Fig. 9. Torque magnitude versus time depending on the connection between upper and lower stators.

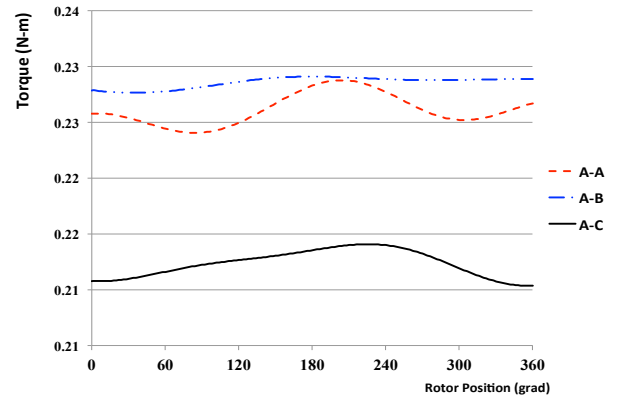


Fig. 10. Torque oscillation depending on rotor position and phase connections.

### VII. CONCLUSION

The determination of phase distribution for optimum design of a full HTS machine using HTS tape assembly was presented. The best results were obtained in the A-B configuration with greater torque at lower ripples. A preliminary 2D model was implemented with good agreement with experimental results in static regime that helped defining the appropriate air gap thickness and phase distribution. This model will be refined to include dynamic processes such as induced current in the rotor and the derivation of time-dependent parameters such as torque and velocity to complete the design and experimental work with more refined analysis.

## REFERENCES

- [1] C.C. Chan, "Axial-field electrical machines-design and applications", *IEEE Trans. On Energy Conversion*, vol. EC-2, pp. 294-300, June 1987.
- [2] S. Huang, J. Luo, F. Leonardi, T.A. Lipo, "A comparison of power density for axial flux machines based on general purpose sizing equations", *IEEE Trans. On Energy Conversion*, Vol. 14, No. 2, pp. 185-192, June 1999.
- [3] J. Lopez, et al, "AC Three-phase axial flux motor with magnetized superconductors", *IEEE Trans. on Applied Superconductivity*, Vol. 17, No. 2, pp. 1633-1635, June 2007.
- [4] J.F. Gieras, R.J. Wang, M.J. Kamper, "Axial flux permanent magnet brushless machines", Kluwer Academic Publishers, ISBN: 1-4020-2661-7, 2004.
- [5] S. Gruss, G. Fuchs, G. Krabbes, P. Verges, P. Schatzle, K. H. Muller, J. Fink, and L. Schultz, "Trapped fields beyond 14 Tesla in bulk YBa<sub>2</sub>Cu<sub>3</sub>O<sub>7-d</sub>", *IEEE Transactions on Applied Superconductivity*, vol. 11, pp. 3720-3723, Mar. 2001.
- [6] Z.Q. Zhu, D. Howe, "Influence of design parameters on cogging torque in permanent magnet machines", *IEEE Transaction on Energy Conversion*, vol 15, No. 4, pp 407-412, Dec. 2000.
- [7] K. Atallah, J. Wang, D. Howe, "Torque-Ripple minimization in modular permanent-magnet brushless machines", *IEEE Transaction on Industry Applications*, Vol. 39, No. 6, pp1689-1695, Dec 2003.
- [8] J. Ogawa, M. Iwamoto, K. Yamagishi, O. Tsukamoto, M. Murakami, M. Tomita, "Influence of AC external magnetic field perturbation on trapped magnetic field in HTS bulk," *Physica C: Superconductivity*, Vo. 386, pp. 26-30, 2002.
- [9] Y. Tsuboi and H. Ohsaki, "Torque Characteristics of a Motor Using Bulki Supercoductors in the Rotor in the transient Phase," *IEEE Transactions on Applied Superconductivity*, Vol. 13, No. 2, 2003.
- [10] Z. Nasiri-Gheidari, H. Lesani, "A survey on axial flux induction motors", *Przeglad Elektrotechniczny*, R. 88NR, pp 300-305, feb. 2012.
- [11] M. Aydin, R. Qu, T.A. Lipo, "Cogging torque minimization technique for multiple-rotor, axial-flux, surface-mounted-PM motors: alternating magnet pole-arcs in facing rotors", *IEEE IAS Annual Meeting Conference*, Salt Lake City, UT, 2003.
- [12] P.J. Masson, M. Breschi, P. Tixador, C.A. Luongo, "Design of HTS Axial Flux Motor for Aircraft Propulsion", *IEEE Transactions on Applied Superconductivity*, Vol. 17, No. 2, pp 1533-1536, June 2007.
- [13] R. Wallace, L. Moran, G. Cea, F. Perez, "Design and construction of medium power axial flux induction motor", *Electrical Machines and Drives, Fifth International Conference, Conf. Publ. No. 341*, pp. 260-265, 11-13 Sept. 1991.
- [14] F. Caricchi, F. Crecimbini, E. Santini, "Axial-flux electromagnetic differential induction motor", *Electrical machines and drives, conference Publication No. 412 IEE*, Sept. 1995.
- [15] M. Valtonen, A. Parviainen, J. Pyrhönen, "Electromagnetic field analysis of 3D structure of axial-flux solid-rotor induction motor", *SPEEDAM 2006, International Symposium on Power Electronics, Electrical Drives, Automation and Motion*, pp. S39-12-S39-16, 2006.
- [16] A. Benoudjit, N. Nait Saïd, "New dual-airgap axial & radial-flux induction motor for on wheel drive electrical propulsion systems", *Power System Technology, Proceeding Powercon '98*, Vol 1, pp. 615-619, 1998.
- [17] W.S. Leung, C.C. Chan, "A new design approach for axial-field electrical machines", *IEEE Trans. On Power Apparatus and Systems*, Vol. PAS-99, No. 4, pp. 1679-1685, July/Aug 1980.
- [18] M. Valtonen, A. Parviainen, and J. Pyrhönen, "Influence of the air-gap length to the performance on an axial-flux induction motor", *Proceeding of the 2008 International Conference on Electrical Machines*, pp. 1-5, 2008.
- [19] M. Trapanese, V. Franzitta, A. Viola, "Design and performance of high temperature superconducting axial flux generator", *IEEE Transaction on Magnetics*, Vol. 49, No. 7, pp 4113-4115, july 2013.
- [20] Z. Nasiri-Gheidari and H. Lesani, "Design optimization of a single-phase axial flux induction motor with low torque ripple", *Electrical Review*, ISSN 0033-2097, pp. 168-172, 2012.
- [21] H. Sugimoto, et al, "Design of an Axial Flux Inductor Type Synchronous Motor With the Liquid Nitrogen Cooled Field and Armature HTS Windings", *IEEE Transaction on Applied Superconductivity*, Vol. 17, No. 2, pp. 1571-1574, June 2007.
- [22] H. Sugimoto, et al, "Development of an Axial Flux Type PM Synchronous Motor With the Liquid Nitrogen Cooled HTS Armature Windings", *IEEE Transaction on Applied Superconductivity*, Vol. 17, No. 2, pp. 1637-1640, June 2007.
- [23] R. H. Engelmann, W. H. Middendorf, "Handbook of electric motors", ISBN: 0-8247-8915-6, 1995.
- [24] A. González-Parada, F. J. Espinosa-Loza and R. Bosch-Tous, "Inductive method for the determination of the critical current  $I_c$  of HTS stators in axial flux configuration", *IEEE Transactions on Applied Superconductivity*, Vol. 22, No. 3, pag. 9500104, Jun. 2012.
- [25] D. Meeker, "Finite Element Method Magnetics": HomePage/ FEMM reference manual, 2010. Online: <http://www.femm.info/wiki/HomePage>
- [26] R. Islam, I. Husain, A. Fardoun, K. McLaughlin; "Permanent-Magnet synchronous motor designs with skewing for torque ripple and cogging torque reduction", *IEEE Transactions on Industry Applications*, Vol. 45, No.1, pag 152-160, jan-feb 2009.